2024 IEEE/RSJ International Conference on Intelligent Robots and Systems (IROS)
October 14-18, 2024. Abu Dhabi, UAE

An Optical Interferometer-based Force Sensor System for Enhancing Precision in Epidural Injection Procedure

Gichan Cho[1], Jintaek Im[1], Hyunjung Kwon[2†], and Cheol Song[1†]

Abstract— **In minimally invasive pain management procedures, precise needle positioning is paramount for effective treatment and patient safety. Traditional techniques like the loss-of-resistance (LOR) method may be insufficient, especially in patients with narrowed epidural spaces. The use of imaging tools such as C-arms carries risks due to radiation exposure for medical professionals. A new system for detecting the epidural space based on optical interferometry is proposed to tackle this issue. Prior research has focused on force measurement systems to identify tissue puncture or rupture. Although mechanical sensors have been utilized, they add bulk and complexity to systems. Optical sensors like Fiber Bragg grating (FBG) and Fabry-Pérot interferometer (FPI) offer stable, high-resolution measurements suitable for complex biological tissues. This study aims to develop a sensor and needle system for epidural injections, incorporating quantitative metrics for validation. An optical interferometer-based force measurement sensor was integrated into a commercial epidural needle, and calibration was performed to establish a correlation between system output and actual force. The system employs a graphical user interface (GUI) to identify puncture points based on abrupt force decreases. A user study involving interventionalists assessed the system's performance by measuring invasive depth and success rates. The user study demonstrated that the proposed sensorized system could detect the puncture with an average success rate of $72.63\ \%$. This study represents a significant advancement toward safer and more precise epidural procedures, addressing critical clinical considerations for practical applications.**

I. Introduction

In minimally invasive procedures, it is essential to position the needle in the targeted biological tissue accurately. Accurate needle placement increases the effectiveness of the treatment and prevents unnecessary damage to the patient. Pain interventional procedures are a standard method of treating pain involving the direct injection of therapeutic drugs into the targeted nerve. As an interventional procedure for back pain, drugs are injected into the epidural space located anatomically between the ligament flavum and the dura [1]. Interventionalists have used the loss-of-resistance (LOR) technique to ensure the needle enters the epidural space [2]. However, the epidural space is considerably constricted, especially in patients with inflammation and stenosis, and the LOR technique alone is insufficient for accurately identifying the puncture moment [3]. Therefore, for a safe procedure, an imaging device called a C-arm has been typically used to monitor the patient's anatomy and the position of the needle. However, radiation from medical imaging devices can pose a significant risk to medical practitioners. Interventionalists conduct a substantial number of procedures and endure prolonged radiation exposure, potentially leading to complications such as skin necrosis on the hands [4] or cataracts [5]. Solving this problem requires a new epidural space detection system that is as reliable as a C-arm or can maintain a safe distance from the imaging device.

The core idea of the previous works is to develop sensor systems that can detect puncture or rupture of the target tissue layer based on force measurements. Measuring and controlling the physical quantities like distance [6–13] and force [14] between the instrument and the tissue are critical concerns in microsurgery and biopsy. For example, there is a study on force-measuring biopsy needles to predict the physical properties of the tissue (e.g., stiffness) when performing a biopsy and use them to reach the target lesion [15]. In [15], a force-measuring needle was realized by combining a mechanical force/torque sensor with a needle mount. However, these mechanical sensors have the disadvantage of making the system large and complicated for microsurgical tools. Therefore, many applications have utilized force measurement systems based on optical interferometers rather than mechanical force sensors.

Optical sensors are characterized by their stable structure and high measurement resolution, which allows them to perform well in complex biological tissues with multiple layers [16]. Fiber Bragg grating (FBG) and Fabry-Pérot interferometer (FPI) are optical interferometers used as force sensors in various studies. In particular, in terms of procedural and diagnostic devices, some systems can be applied to microneedles in direct contact with thin membranes [17], the sclera [18], capillaries [19], and retina [20] to measure and control force to prevent secondary damage. Diagnostic systems have also been proposed for biopsy needles to analyze tissue stiffness and predict diseases like cancer [21]. These studies focus on the development of sensors for force measurement. In contrast, epidural works primarily concentrate on implementing a system that detects puncture of the ligament flavum based on changes in the measured force profile [22–24]. However, since most of the previous studies were conducted by non-experts, it is necessary to conduct further analysis on crucial clinical aspects, such as

† Corresponding author
[1]Department of Robotics and Mechatronics Engineering, DGIST, Daegu 42988, South Korea (cgch-dgist18, wlsehd23, csong)@dgist.ac.kr
[2]Department of Anesthesiology and Pain Medicine, Seoul Asan Medical Center, Seoul 05505, South Korea kwonhj@amc.seoul.kr
*This work was supported by the Technology Innovation Program (20023168, Development of clinician collaborative robot platform technology for 3 types of pain interventional procedures based on crossdrug handler and instrument modules) funded by the Ministry of Trade of Trade, Industry & Energy(MOTIE, Korea).

the statistical success rate and invasive depth after puncturing the ligament flavum.

The contribution point of this work is the development of a sensor and needle system for epidural injection, along with the quantitative metrics to validate the performance of the proposed method. We developed an optical interferometer-based force measurement sensor and applied it to a commercial epidural needle to form a sensorized needle system. We also performed calibration between the output of the system and the actual acting force. The force between the biological tissue and the sensorized needle was defined as the penetration force, and the graphical user interface (GUI) was configured to recognize the point where the force instantaneously decreases as a puncture. To verify the performance of the proposed system, we conducted a user study by recruiting interventionalists. In the user study, the invasive depth was measured immediately after the needle stopped advancing, and the success rate was calculated by recording the participants' test successes and failures.

II. System Design and Method

This section presents the design and development of an optical force sensor and needle system for epidural injections utilizing a sensorized needle. We designed the hardware and GUI to apply to commercially available epidural needles and allow users to intuitively understand the principle of the system and use it easily.

A. Optical force sensor

Previous studies targeting epidural injections have developed sensors based on the principle of optical systems called Fiber Bragg grating (FBG) or Fabry-Pérot (FPI) to measure the force acting on the needle. Both optical systems are characterized by high durability and measurement resolution. However, compared to FPI, FBG has a much higher sensitivity to temperature changes. The high sensitivity on the temperature poses challenges in accurately measuring the desired parameter due to the fluctuations in sensor values induced by temperature variations. Therefore, additional temperature compensation is required in this case. Furthermore, FBGs are structurally more complicated than FPIs. Considering these points, we adapted the structure of the FPI to develop a force measurement sensor.

The optical system is organized as a common-path interferometer, which is similar to optical coherence tomography [25–27], as shown in Fig. 1(a). The laser beam source from the laser device is transmitted to the sensor through a beam splitter, and the interference signal generated by the sensor travels through the beam splitter to the detector. The force sensor based on the FPI structure forms a small cavity between the single-mode fiber and the reflector. Therefore, light is reflected from the end of the optical fiber and the reflector's surface, respectively, as shown in Fig. 1(b). An optical path length (OPL) difference between the two parallel lights depends on the cavity length. In an optical system, the difference in the OPL of two lights induces interferometric signal, and we can use it to measure the external force The

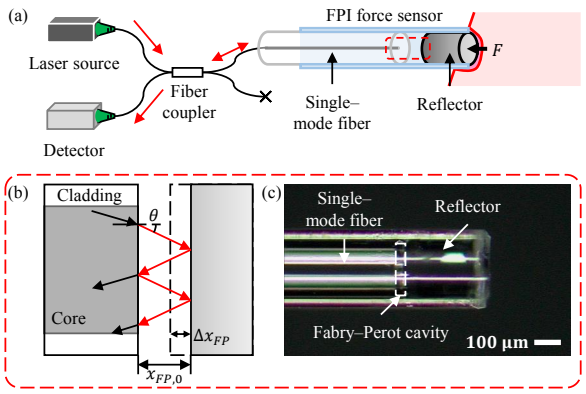

Fig. 1. Fabry-Pérot interferometer-based force sensor: (a) optical configuration of Fabry-Pérot interferometer force sensor, (b) Fabry-Pérot cavity length change, (c) implemented force sensor.

OPL, Δ and the phase shift $\Delta\phi_{shift}$ of the interference signal can be expressed as follows [28]:

$$\Delta = 2nx_{FP}\cos\theta = 2n(x_{FP,0} + \Delta x_{FP})\cos\theta \quad (1)$$

$$\Delta\phi_{shift} = (\frac{2\pi}{\lambda})\Delta = \frac{4\pi n(x_{FP,0} + \Delta x_{FP})\cos\theta}{\lambda} \quad (2)$$

where n is the refractive index, λ is the wavelength, θ is the incidence angle, x_{FP} is the length of the Fabry-Pérot cavity, and n_{air} is the refractive index of air.

An external force acts on the FPI sensor, causing a change in cavity length equal to Δx_{FP}. According to Eqs. 1 and 2, a minimal change in the cavity length leads to a phase shift of the interference signal, so we can estimate the force acting proportionally to $\Delta\phi_{shift}$.

B. Sensorized needle system

During the needle insertion process, the FPI force sensor fabricated in Sec. II-A above was applied to a commercial epidural needle to construct a sensorized needle to measure the force acting on the needle. As shown in Fig. 2(b), the sensor is inserted into the inner cannula of the needle and attached to its wall. This design allows for space within the needle for the passage of medication while simultaneously measuring the contact force with biological tissue. In pain intervention procedures, epidural needles of various sizes are used, ranging from 17G to 25G, depending on the procedure site and process. However, in this study, we selected a 22G size needle that is widely used in epidural injections. Moreover, since the inner cannula of the 22G needle has a diameter of 410 μm, we were able to fully insert an optical force sensor module with a much smaller diameter into the needle.

According to previous studies on the interaction between needles and biological tissue, the needle experiences two different types of forces from the tissue during insertion [29]. In contrast, in our study, the needle's penetration force was minimally affected by cutting force or friction, and the contact force was clearly measured when the sensor was in direct contact with the tissue. Additionally, the sensorized needle

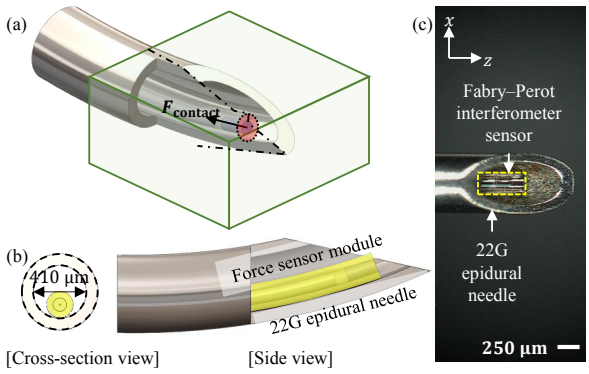

Fig. 2. Proposed sensorized needle system: (a) penetration force measurement mechanism, $F_{contact}$: contact force, (b) configuration and dimension of sensorized needle, (c) implemented sensorized needle system.

measures the contact force in the axial direction directly at the needle tip. Therefore, the measurement performance of the axial force is not significantly influenced by lateral force changes caused by needle bending. Consequently, the penetration force $F_{penetration}$ is equal to contact force.

III. System Calibration and Validation

As detailed in Sec. II, the force sensor and needle system produce a sensor value proportional to the external force applied, which is then presented to the user through the GUI.

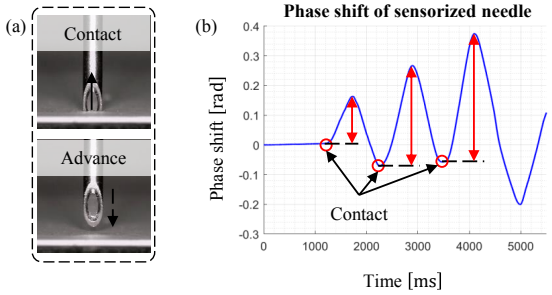

Fig. 3. Phase shift of sensoirzed needle system: (a) contact and non-contact situation of needle, (b) phase shift result according to the magnitude of contact force.

Our proposed system functions as a force measurement sensor by analyzing the optical interferometer signal. As depicted in the preliminary experiment in Fig. 3, the sensorized needle discerns the presence of contact between the needle and the sample via phase shift changes and exhibits output value proportional to contact force magnitude.

A. Penetration force-phase shift calibration

The proposed sensorized needle system is designed to be sensitive to the force in the direction of the penetration depth of the needle, i.e., in the axial direction. The output value of the sensor, $\Delta\phi_{shift}$, was described in Sec. II-A as Eq. 2. Therefore, the difference of the sensor value $\Delta\phi_{shift}^{diff}$ can be expressed as follows:

$$\Delta\phi_{shift}^{diff} = \frac{4\pi n \Delta x_{FP} \cos\theta}{\lambda} \tag{3}$$

The difference solely relies on the linear deformation of the FP cavity length caused by external force, establishing a proportional relationship between force and phase shift, as follows:

$$\Delta F_{penetration} = C_{axial} \Delta\phi_{shift}^{diff} \tag{4}$$

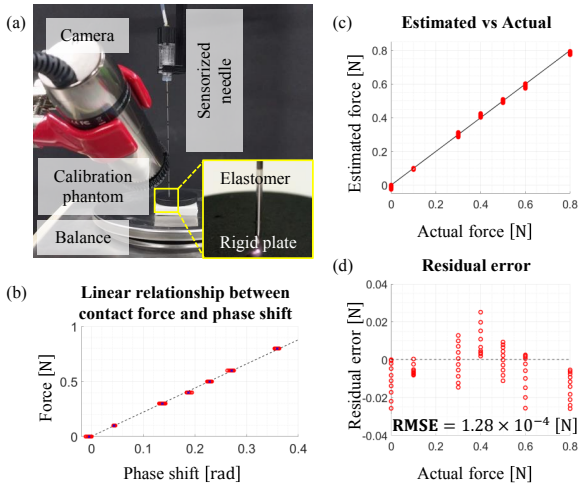

Fig. 4. Force-phase shift calibration and estimation: (a) sensorized needle calibration setup, (b) linear relationship between force and phase shift (c) estimated penetration force versus actual force value, (d) residual error of estimation.

where C_{axial} is the mapping coefficient determined by the calibration procedure. For the calibration, the force was applied to the sensorized needle at regular intervals, recording 10 data points. We used a linear stage and high-precision balance for the calibration setup, as shown in Fig. 4(a). The sensorized needle, attached to the linear stage, gradually moves closer to the balance, increasing penetration force incrementally. To address errors caused by needle tip slippage on the balance plate, we employed a sample using elastomer and rigid plate, as outlined in [18]. The precision electronic balance used in our experiment has a measurement precision of 0.0001 g. Utilizing the relationship between weight and force (approximately 1.00 g $= 10.00$ mN), we determined the force acting on the sensorized needle from the balance's measurement. Using the linear stage, we applied the force to the calibration phantom at 0.1 N. Fig. 4(b) illustrates the linear relationship between penetration force and phase shift. Under these conditions, values of the actual force measured by the balance that differed from the reference by more than 0.03 N were considered outliers. After excluding the outlier data, the linear mapping coefficient C_{axial} was found to be $2.19\ \frac{\text{N}}{\text{rad}}$. Subsequently, using the axial force coefficient, we performed cross-validation by comparing the estimated force meaured by the FPI sensor with the actual force values.

The estimated penetration force versus their actual force and residual error are shown in Fig. 4(c) and (d), respectively. As a result of the validation, the penetration force measured

by the sensorized needle has a good agreement with the actual value. The estimated values' root mean square (RMS) error was 1.28×10^{-4} N.

B. Resolution of sensorized needle system

The needle system's force measurement resolution was evaluated, revealing an axial resolution of approximately 0.05 N, which is ten times better than previous studies' 0.50 N [24]. This suggests significantly improved precision for force measurements in living tissue.

IV. System Performance Evaluation

This section describes a user study conducted on clinicians and its results. It was planned to compare the clinical performance of the sensorized needle system and the GUI implemented and calibrated in Sec. II and Sec. III. A user study was conducted by recruiting a total of 23 interventionalists. Fig. 5 shows the outline of the user study conducted in this study and the experimental setup, and the anesthetists who participated in the experiment are described in the Tab. I.

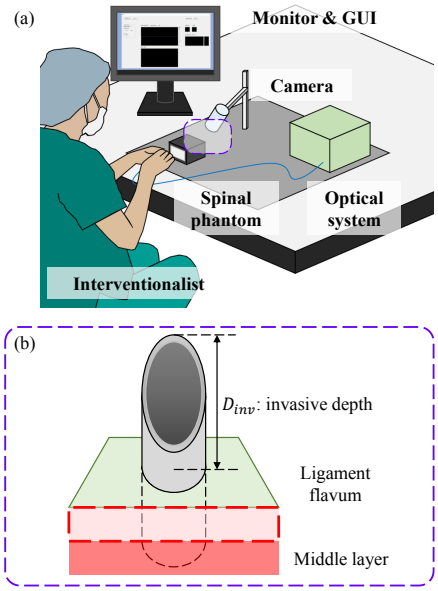

Fig. 5. Systematic setup for user study with interventionalists: (a) user study progress and overview, (b) definition of needle invasive depth D_{inv}.

As shown in Fig. 5(a), interventionalists detect punctures on a custom spinal phantom. The puncture detection task was performed using the existing loss of resistance technique and the developed sensorized needle system. At this time, a camera installed right above the phantom is used to measure needle penetration and the invasive depth of the needle. During the user study, the doctors relied only on their senses and the graphical user interface (GUI) of the sensorized needle. The usability of the custom phantom was verified by performing the existing loss of resistance technique five times, and five simple training sessions on the sensorized needle and GUI were conducted before starting the experiment. After training, the subjects were asked to perform ten puncture detection tasks using a sensorized needle. During this process, the inspector measured the force profile during needle penetration, the invasive depth of the needle, and the task's success rate. After all experimental processes were completed, a survey was conducted on the participating interventionalists to receive overall feedback on the system.

A. Spinal phantom design and evaluation

We developed an anatomically modeled epidural phantom for user studies with the Phantom. Before reaching the epidural space, the needle traverses multiple layers of biological tissue, including skin, mesenchyme (muscles and ligaments), and ligament flavum. The mesenchymal layer comprises supraspinous and interspinous tissues. The ligament flavum is the most rigid tissue before the epidural space. The study aims to detect ligament flavum puncture and accurately position the needle in the epidural space.

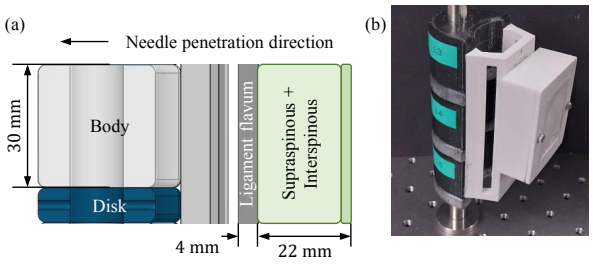

Fig. 6. Custom spinal phantom for user study: (a) spinal phantom design and dimension based on anatomical structure, (b) implemented phantom.

Fig. 6(a) illustrates our custom epidural phantom design, featuring a representation of the canal for the spinal nerve pathway. This model defines the epidural space as the canal area excluding the nerves. The ligament flavum, our target layer, demonstrates varied characteristics influenced by age, gender, and health conditions. We referenced relevant studies, including [30], which explored ligament flavum thickness across cadaveric species to determine its physical thickness. Based on statistical analysis, the thickness of ligament flavum typically ranges from 2.50 mm to 4.00 mm, and it increases with age. Considering this trend, we established the ligament flavum thickness for our custom phantom at 4.00 mm. We fabricated specimens using silicone-based polymer, selected for its texture akin to ligament flavum and comparable hardness [31]. Before commencing experiments with the sensorized needle, all participating interventionalists assessed the suitability of the epidural phantom. They each performed the LOR technique on the phantom five times to gauge its resemblance to natural biological tissue. The feedback revealed that while the phantom was somewhat less rigid than actual ligament flavum, all interventionalists deemed it highly suitable for LOR.

B. Puncture detection task

The process of epidural needle penetration can be divided into four main phases [19], depicted in Fig. 7(a)-(d) based on the force profile.

TABLE I

INFORMATION ON PARTICIPATING INTERVENTIONALISTS.

	Gender	Age	Rank	Session number	Clinical experience(n)
Subject 01	female	30s	Professor	2	$1000 \leq n$
Subject 02	male	40s	Professor	2	$1000 \leq n$
Subject 03	female	20s	Resident	0	$50 \leq n < 100$
Subject 04	female	30s	Fellow	1	$100 \leq n < 300$
Subject 05	male	30s	Fellow	4	$1000 \leq n$
Subject 06	male	40s	Intern	0	$n = 0$
Subject 07	female	20s	Intern	0	$n = 0$
Subject 08	female	30s	Professor	0	$100 \leq n < 300$
Subject 09	male	up to 50s	Professor	2	$1000 \leq n$
Subject 10	male	30s	Fellow	4	$100 \leq n < 300$
Subject 11	male	30s	Professor	1	$1000 \leq n$
Subject 12	male	40s	Professor	0	$1000 \leq n$
Subject 13	male	up to 50s	Professor	3	$1000 \leq n$
Subject 14	female	20s	Resident	0	$100 \leq n < 300$
Subject 15	female	20s	Resident	0	$0 < n < 10$
Subject 16	male	30s	Fellow	4	$1000 \leq n$
Subject 17	male	30s	Resident	0	$100 \leq n < 300$
Subject 18	male	20s	Resident	0	$50 \leq n < 100$
Subject 19	male	30s	Resident	0	$50 \leq n < 100$
Subject 20	male	30s	Fellow	0	$50 \leq n < 100$
Subject 21	female	20s	Resident	0	$50 \leq n < 100$
Subject 22	male	20s	Resident	0	$0 < n < 10$
Subject 23	male	40s	Professor	0	$1000 \leq n$

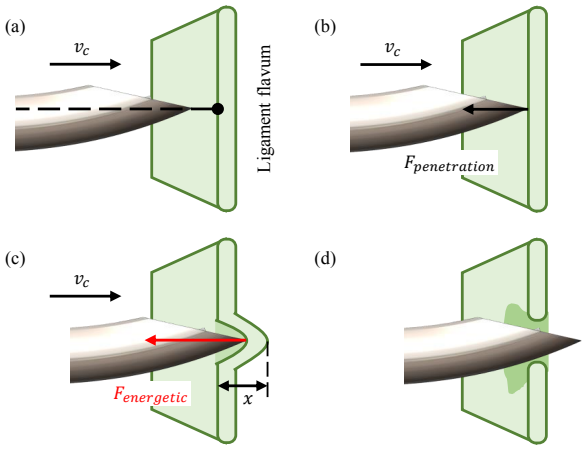

Fig. 7. Needle insertion mechanism: , (a) needle approaches to tissue with constant velocity, (b) needle contacts with tissue surface, (c) deformation of tissue layer occurs due to the needle insertion, (d) tissue layer is punctured after penetration force reach to the energetic threshold of tissue.

As the needle contacts the tissue at a constant velocity, force begins to act, increasing linearly with tissue deformation until reaching an energetic threshold. Upon tissue puncture or rupture, the force decreases instantaneously. The sensorized needle system employs a GUI to display the measured force profile to users. In the user study, interventionalists were tasked with detecting punctures by halting needle advancement upon observing an instantaneous drop in the displayed force graph.

C. Success rate and effectiveness

Accurately positioning the epidural needle without puncturing the dura requires careful consideration of the needle penetration depth, D_{inv}. Locating the epidural space presents challenges due to the close adherence of the ligament flavum and dura mater, with fat filling the remaining space. Interventionalists prioritize even the smallest space for procedural safety. Clinically, the maximum achievable epidural space size ranges from 3.00 mm (cervical) to 5.00 mm (lumbar), but inflammation and stenosis in patients can further reduce this. In this study, assuming a 5.00 mm epidural space size, invasive depth was measured using a camera to observe the phantom's interior. As detailed in the Tab. II, *success* was defined as an invasive depth between 0.00 mm and 5.00 mm, ensuring needle entry into the epidural space without dural contact. The invasive depth evaluation used recorded camera images post-trials. Nineteen participants were assessed, with four excluded due to difficulty determining needle depth from the video.

TABLE II

SUCCESS/FAILURE OF PUNCTURE DETECTION TASK.

Invasive depth [mm]	Success / Fail
$D_{inv} < 0.00$	Fail
$0.00 \leq D_{inv} < 5.00$	Success
$5.00 \leq D_{inv}$	Fail

Fig. 8 displays invasive depth, mean, and variance across ten trials per participant. During the puncture detection task with the sensorized needle, 16 participants had invasive depths below 5.00 mm.

Based on this, we assessed the success rate. Fig. 9 shows that 13 participants achieved a success rate of 70.00 % or higher, with an average success rate of 72.63 %.

D. Penetration force profile using injection system

From the user study, we recorded the force profile measured by the sensorized needle. According to needle dynamics, corresponding peaks should appear when a puncture occurs in each layer of the phantom. We analyzed the force

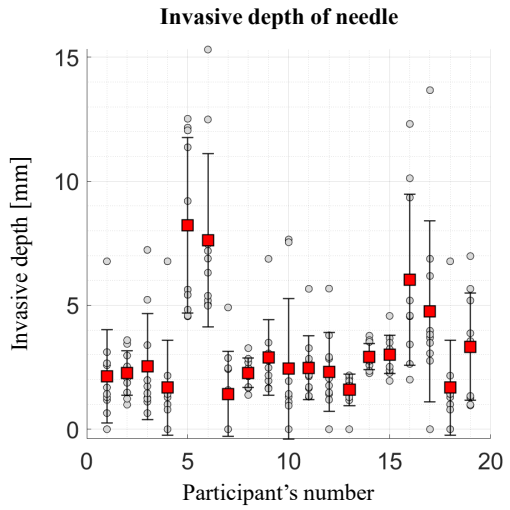

Fig. 8. Needle invasive depth from user study: (a) definition of needle invasive depth D_{inv}, (b) needle invasive depth for each participants and trials.

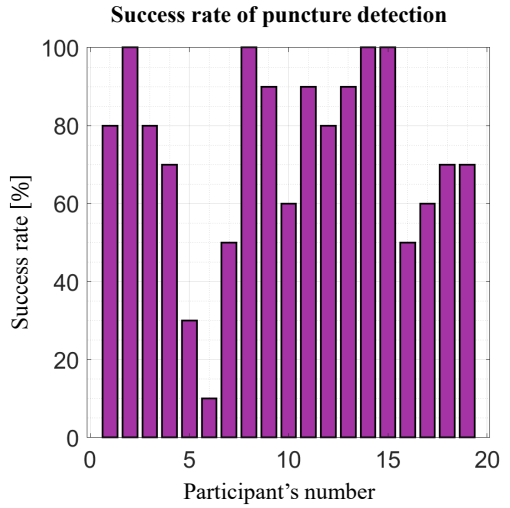

Fig. 9. Success rate for each puncture detection task: user study results for 19 participants, excluding experimental data from 4 whose invasive depth was challenging to confirm accurately. The average success rate was calculated to be approximately 72.63 %.

profiles for the success cases of participants with a success rate of 70.00 % or higher.

During manual penetration, the system's force profile (blue line, Fig. 10) exhibited two prominent peaks spanning from skin to ligament flavum. The penetration force increased up to the energetic threshold of each layer and then precipitously decreased upon puncture occurrence. In particular, we observed a notable measurement of the puncture peak of the target layer compared to the other parts of the custom phantom. Through this result, we have demonstrated the ease of detecting puncture of the ligament flavum using a sensorized needle based on force.

Before implementing the automated injection system, we

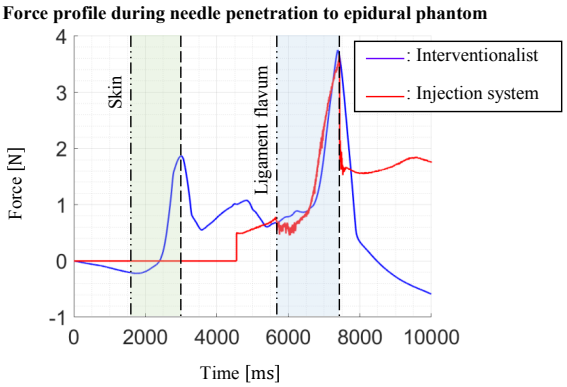

Fig. 10. Penetration force profile during sensorized needle insertion: two puncture peaks (skin and ligament flavum) from manual insertion (blue line) by interventionalists, single puncture peak (ligament flavum) from needle penetration by injection system (red line).

conducted a preliminary test to obtain a force profile with distinct puncture peaks similar to those observed during manual insertion. The injection system was implemented using a motorized linear stage. Due to the short travel distance of the motorized linear stage (Thorlabs, Z812B, 12.0 mm travel length), all external layers of the custom phantom were removed. With open-loop control, the linear stage inserts the needle into the target layer at a steady velocity. In the force profile obtained from the motorized linear stage experiment (red line, Fig. 10), a prominent puncture point was evident, and compared to the manual procedure, a more pronounced decrease in force was noted. Experimental results represented peaks that could predict the puncture of the ligament flavum for both manual and automatic insertions. Additionally, a more pronounced force drop was observed during motorized stage-based penetration. Moreover, with the capability to precisely control the needle advancement velocity, it is anticipated that improved predictive results for puncture will be achieved compared to manual insertion.

V. Conclusion and Future Work

Detecting puncture or rupture of soft tissue is crucial for estimating the needle's location during epidural injection. By measuring the force acting on the needle, it is possible to determine whether the needle has penetrated the ligament flavum and accessed the epidural space. Our study develops an optical force sensor with a Fabry-Perot interferometer and motorized needle injection system. In addition, we performed a puncture detection task using a custom epidural phantom with 23 interventionalists and evaluated their success rate and invasive depth. The proposed sensorized needle is demonstrated to assist in safe epidural injection.

In future work, we plan to optimize the proposed system based on various opinions gathered from interventionalists and implement optimal control algorithms for automated robot-assisted injections. Furthermore, this system is anticipated to be applied not only to epidural injections but also to various microsurgeries requiring precise force measurements, such as brain and laparoscopic surgeries.

REFERENCES

[1] M. C. Bicket, A. Gupta, C. H. Brown IV, and S. P. Cohen, "Epidural injections for spinal pain: a systematic review and meta-analysis evaluating the "control" injections in randomized controlled trials," *Anesthesiology*, vol. 119, no. 4, pp. 907–931, 2013.

[2] J. Y. Lee, S. M. Lee, W. S. Sim, H. J. Ahn, M. H. Park, H. Y. Lim, S. H. Lee, Y. R. Kim, Y. I. Kim, and Y. J. Bang, "False loss of resistance in cervical epidural injection: the loss of resistance technique compared with the epidrum guidance in locating epidural space," *Pain physician*, vol. 19, no. 3, p. 131, 2016.

[3] W. S. Bartynski, S. Z. Grahovac, and W. E. Rothfus, "Incorrect needle position during lumbar epidural steroid administration: inaccuracy of loss of air pressure resistance and requirement of fluoroscopy and epidurography during needle insertion," *American journal of neuroradiology*, vol. 26, no. 3, pp. 502–505, 2005.

[4] D. M. Shim, Y. M. Kim, S. K. Oh, C. M. Lim, and B. T. Kown, "Radiation induced hand necrosis of an orthopaedic surgeon who had treated a patient with fluoroscopy-guided spine injection," *Journal of the Korean Orthopaedic Association*, vol. 49, no. 3, pp. 250–254, 2014.

[5] S. Jacob, S. Boveda, O. Bar, A. Brézin, C. Maccia, D. Laurier, and M.-O. Bernier, "Interventional cardiologists and risk of radiation-induced cataract: results of a french multicenter observational study," *International journal of cardiology*, vol. 167, no. 5, pp. 1843–1847, 2013.

[6] C. Song, P. L. Gehlbach, and J. U. Kang, "Swept source optical coherence tomography based smart handheld vitreoretinal microsurgical tool for tremor suppression," in *2012 Annual International Conference of the IEEE Engineering in Medicine and Biology Society*, 2012, pp. 1405–1408.

[7] C. Song, D. Y. Park, P. L. Gehlbach, S. J. Park, and J. U. Kang, "Fiber-optic oct sensor guided "smart" micro-forceps for microsurgery," *Biomed. Opt. Express*, vol. 4, no. 7, pp. 1045–1050, Jul 2013.

[8] C. Song, P. L. Gehlbach, and J. U. Kang, "Ball lens fiber optic sensor based smart handheld microsurgical instrument," in *Optical Fibers and Sensors for Medical Diagnostics and Treatment Applications XIII*, I. Gannot, Ed., vol. 8576, International Society for Optics and Photonics. SPIE, 2013, p. 85760I.

[9] H. C. Park, C. B. Yeo, P. L. Gehlbach, and C. Song, "Development of the dual smart micro-surgical system using common-path swept source optical coherence tomography," in *2015 37th Annual International Conference of the IEEE Engineering in Medicine and Biology Society (EMBC)*, 2015, pp. 5–8.

[10] D. Koo, H.-C. Park, P. L. Gehlbach, and C. Song, "Development and preliminary results of bimanual smart micro-surgical system using a ball-lens coupled oct distance sensor," *Biomed. Opt. Express*, vol. 7, no. 11, pp. 4816–4826, Nov 2016.

[11] C. Yeo, H.-C. Park, S. Jang, P. L. Gehlbach, and C. Song, "Dual optical coherence tomography sensor guided, two-motor, horizontal smart micro-scissors," *Optics letters*, vol. 41, no. 20, pp. 4723–4726, 2016.

[12] J. Im and C. Song, "Oblique injection depth correction by a two parallel oct sensor guided handheld smart injector," *Biomed. Opt. Express*, vol. 12, no. 2, pp. 926–939, Feb 2021.

[13] J. Im, S. Park, and C. Song, "Handheld motorized injection system with fiber-optic distance sensors and adaptive time-delay controller," *Int. J. Optomechatronics*, vol. 18, no. 1, p. 2299023, 2024.

[14] W. T. Latt, R. C. Newton, M. Visentini-Scarzanella, C. J. Payne, D. P. Noonan, J. Shang, and G. Z. Yang, "A hand-held instrument to maintain steady tissue contact during probe-based confocal laser endomicroscopy," *IEEE Transactions on Biomedical Engineering*, vol. 58, no. 9, pp. 2694–2703, 2011.

[15] L. Barbé, B. Bayle, M. de Mathelin, and A. Gangi, "In vivo model estimation and haptic characterization of needle insertions," *The International Journal of Robotics Research*, vol. 26, no. 11-12, pp. 1283–1301, 2007.

[16] J. Im and C. Song, "Oblique injection depth correction by a two parallel oct sensor guided handheld smart injector," *Biomed. Opt. Express*, vol. 12, no. 2, pp. 926–939, 2021.

[17] S. Elayaperumal, J. H. Bae, B. L. Daniel, and M. R. Cutkosky, "Detection of membrane puncture with haptic feedback using a tip-force sensing needle," in *2014 IEEE/RSJ International Conference on Intelligent Robots and Systems*. IEEE, 2014, pp. 3975–3981.

[18] T. Zhang, B. Chen, and S. Zuo, "A novel 3-dof force sensing microneedle with integrated fiber bragg grating for microsurgery," *IEEE Transactions on Industrial Electronics*, vol. 69, no. 1, pp. 940–949, 2021.

[19] A. Alamdar, N. Patel, M. Urias, A. Ebrahimi, P. Gehlbach, and I. Iordachita, "Force and velocity based puncture detection in robot assisted retinal vein cannulation: In-vivo study," *IEEE Transactions on Biomedical Engineering*, vol. 69, no. 3, pp. 1123–1132, 2021.

[20] X. Liu, I. I. Iordachita, X. He, R. H. Taylor, and J. U. Kang, "Miniature fiber-optic force sensor based on low-coherence fabry-pérot interferometry for vitreoretinal microsurgery," *Biomedical optics express*, vol. 3, no. 5, pp. 1062–1076, 2012.

[21] D. Uzun, O. Ülgen, and Ö. Kocatürk, "Optical force sensor with enhanced resolution for mri guided biopsy," *IEEE Sensors Journal*, vol. 20, no. 16, pp. 9202–9208, 2020.

[22] A. Beisenova, A. Issatayeva, D. Tosi, and C. Molardi, "Fiber-optic distributed strain sensing needle for real-time guidance in epidural anesthesia," *IEEE Sensors Journal*, vol. 18, no. 19, pp. 8034–8044, 2018.

[23] B. Carotenuto, A. Micco, A. Ricciardi, E. Amorizzo, M. Mercieri, A. Cutolo, and A. Cusano, "Optical guidance systems for epidural space identification," *IEEE Journal of Selected Topics in Quantum Electronics*, vol. 23, no. 2, pp. 371–379, 2016.

[24] Z. Mo, J. Li, and W. Xu, "Tactile needle probe for minimally invasive tissue identification during epidural space insertion," *Optik*, vol. 242, p. 167285, 2021.

[25] D. Huang, E. A. Swanson, C. P. Lin, J. S. Schuman, W. G. Stinson, W. Chang, M. R. Hee, T. Flotte, K. Gregory, C. A. Puliafito, and J. G. Fujimoto, "Optical coherence tomography," *Science*, vol. 254, no. 5035, pp. 1178–1181, 1991.

[26] C. Song, M. Ahn, and D. Gweon, "Polarization-sensitive spectral-domain optical coherence tomography using a multi-line single camera spectrometer," *Opt. Express*, vol. 18, no. 23, pp. 23 805–23 817, Nov 2010.

[27] D. Wang, J. Zhang, L. Liu, Z. Yan, P. Wang, Y. Ding, and H. Xie, "Application of oct for osteonecrosis using an endoscopic probe based on an electrothermal mems scanning mirror," *International Journal of Optomechatronics*, vol. 15, no. 1, pp. 87–96, 2021.

[28] M. R. Islam, M. M. Ali, M.-H. Lai, K.-S. Lim, and H. Ahmad, "Chronology of fabry-perot interferometer fiber-optic sensors and their applications: a review," *Sensors*, vol. 14, no. 4, pp. 7451–7488, 2014.

[29] A. M. Okamura, C. Simone, and M. D. O'leary, "Force modeling for needle insertion into soft tissue," *IEEE transactions on biomedical engineering*, vol. 51, no. 10, pp. 1707–1716, 2004.

[30] J. Abbas, K. Hamoud, Y. M. Masharawi, H. May, O. Hay, B. Medlej, N. Peled, and I. Hershkovitz, "Ligamentum flavum thickness in normal and stenotic lumbar spines," *Spine*, vol. 35, no. 12, pp. 1225–1230, 2010.

[31] G. Capogna, A. Coccoluto, E. Capogna, and A. Del Vecchio, "Objective evaluation of a new epidural simulator by the compuflo® epidural instrument," *Anesthesiology Research and Practice*, vol. 2018, 2018.